Tabular data listings and additional details of the artificial thickening design, experimental apparatus, measurement techniques, and qualification tests are given by Ligrani.[4]

Acknowledgments

The authors gratefully acknowledge the many helpful comments and suggestions of J. P. Johnston with regard to this research effort. This work was supported by the Office of Naval Research, Contracts N00014-67-A-0112-0072 and N00014-76-C-0532. The authors wish to thank J. Patton for his support.

References

[1] Peterka, J.A. and Cermak, J.E., "Simulation of Atmospheric Flows in Short Wind Tunnel Test Sections," CER73-74JAP-JEC32, Fluid Mechanics Program, Colorado State University, June 1974.

[2] Otten, III, L.J., and Van Kuren, J.T., "Artificial Thickening of High Subsonic Mach Number Boundary Layers," *AIAA Journal*, Vol. 14, Nov. 1976, pp. 1528-1533.

[3] Klebanoff, P.S. and Diehl, Z.W., "Some Features of Artificially Thickened Fully Developed Turbulent Boundary Layers with Zero Pressure Gradient," NACA Rept. 1110, 1952.

[4] Ligrani, P.M., Moffat, R.J., and Kays, W.M., "The Thermal and Hydrodynamic Behavior of Thick, Rough-Wall, Turbulent Boundary Layers," Rept. No. HMT-29, Thermosciences Div., Dept. of Mechanical Engineering, Stanford University, 1979.

[5] Schultz-Grunow, F., "New Frictional Resistance Law for Smooth Plates," NACA TM 986, Sept. 1941.

[6] Clauser, F.H., "Turbulent Boundary Layers in Adverse Pressure Gradients," *Journal of the Aeronautical Sciences*, Vol. 21, 1954, p. 91.

[7] Laufer, J., "The Structure of Turbulence in Fully Developed Pipe Flow," NACA Rept. 1174, 1954.

[8] Clauser, F.H., "The Turbulent Boudnary Layer," *Advances in Applied Mechanics*, Vol. IV, Academic Press, New York, 1956, pp. 1-51.

[9] Coles, D., "The Law of the Wake in the Turbulent Boundary Layer," *Journal of Fluid Mechanics*, Vol. 1, 1956, pp. 191-226.

[10] Klebanoff, P.S., "Characteristics of Turbulence in a Boundary Layer with Zero Pressure Gradient," NACA TN 3178, 1954.

[11] Moffat, R.J. and Kays, W.M., "The Turbulent Boundary Layer on a Porous Plate: Experimental Heat Transfer with Uniform Blowing and Suction," Rept. No. HMT-1, Thermosciences Div., Dept. of Mechanical Engineering, Stanford University, 1967.

Real-Time Optical Measurement of Time-Dependent Shock Position

M. Sajben* and R.C. Crites†

McDonnell Douglas Corporation, St. Louis, Mo.

Introduction

IN the study of unsteady flows that contain oscillating shocks, it is desirable to obtain a real-time analog signal representing the streamwise position of the shock. Such a signal permits recording of shock position simultaneously with other time-dependent data (pressures, velocities, etc.). Simultaneous recording insures a precisely indexed time base for all signals and allows reliable computation of joint statistical properties, such as cross-correlations or conditionally averaged flow properties, using shock position as the trigger signal. In addition, the availability of on-line display of time-mean shock position provides the experimental convenience of taking data at preset shock positions.

Description of Apparatus

In a recent experimental study,[1] the need just outlined was met by incorporating a line-scan television camera in the conventional shadowgraph system of the flow facility, and

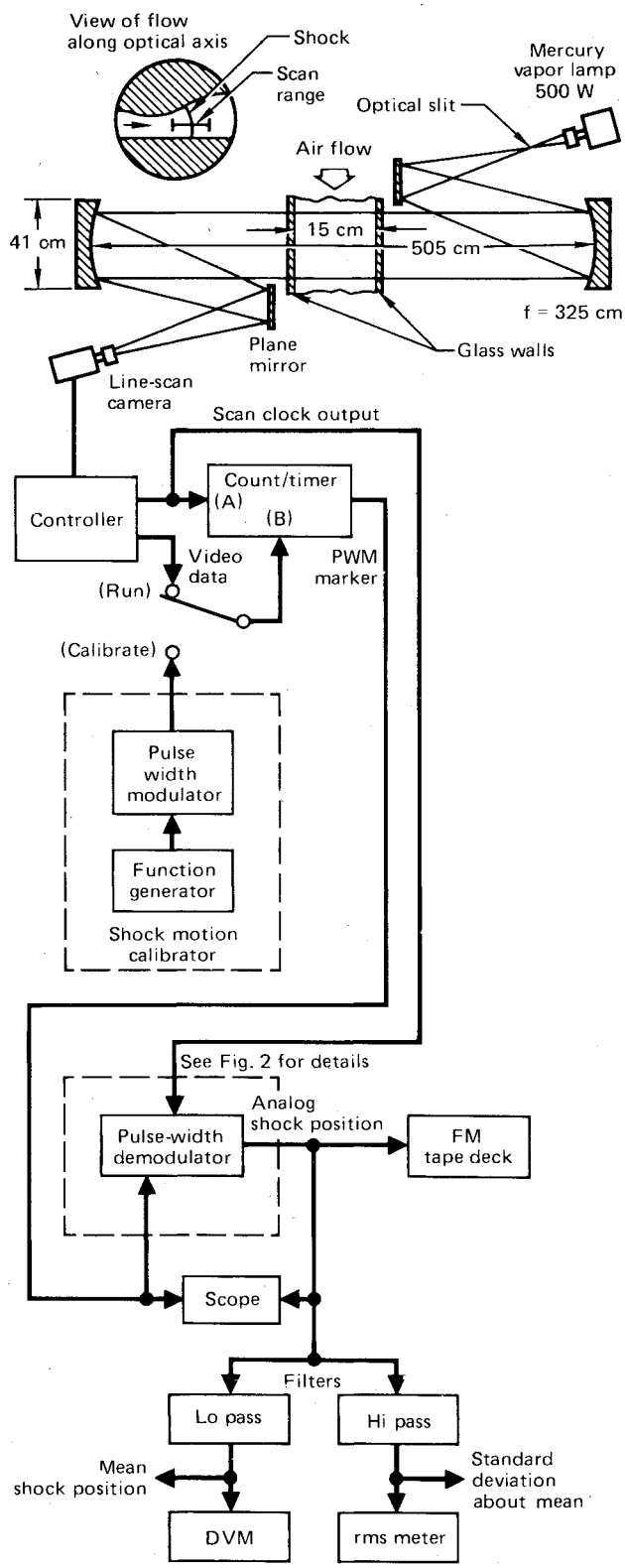

Fig. 1 Layout of shadowgraph system and schematic of electronics for line-scan data processing.

Received Jan. 8, 1979.

Index categories: Shock Waves and Detonations; Research Facilities and Instrumentation.

*Senior Scientist, McDonnell Douglas Research Laboratories. Associate Fellow AIAA.

†Senior Engineer, McDonnell Aircraft Company. Member AIAA.

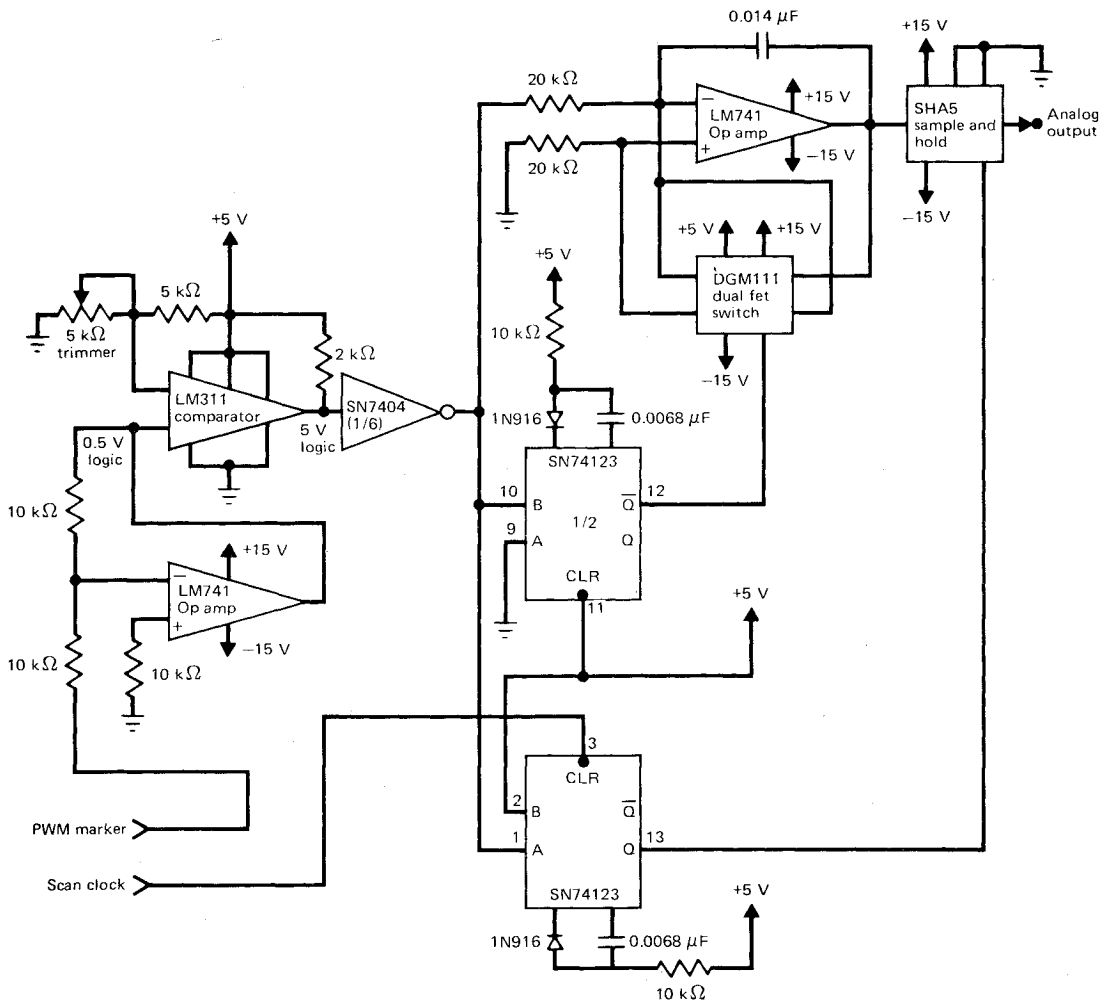

Fig. 2 Pulse width modulation (PWM) decoding circuit.

complementing it with simple image-processing electronics. The system produced an analog shock-position signal which was recorded on FM magnetic tape simultaneously with 12 other analog pressure signals and 1 time code signal as a time-base reference. Alternately, the system was used to provide real-time displays of mean-shock position and shock-fluctuation rms signals. The principal component of the system is a line-scan camera (Reticon Corp. model LC256V with RS605 controller), containing a linear array of photodiodes (pixels) with 25.4 μm spacing. The camera serially multiplexes the pixel array to produce an output representing the intensity distribution of light falling on the array. The camera is capable of scanning at rates adjustable up to $f_{s,\max} = 1.05 \times 10^6$ pixels/s. The number of frames per second depends on N, the number of pixels in the array: $f_f \cong f_s/N$. The camera chosen had $N = 256$ pixels and a maximum frame rate of 3.9 kHz. Since the shock oscillation frequency seldom exceeded 200 Hz in the flow under study, this frame rate was satisfactory.

The camera also provides auxiliary outputs necessary for interim processing of the video output, such as a scan clock pulse at the beginning of each scan. It is also equipped with an internal comparator which sets a data flag if the light intensity drops below an adjustable reference value during any given scan. The flag is reset at the end of each scan.

The camera was incorporated into a shadowgraph system to scan the flow in the streamwise (horizontal) direction; the shock image was a dark line, normal to the sensor array (Fig. 1). The system sensed the intersection of the scan line and the upstream edge of the shock; temporal shock shape changes were sufficiently small to consider the location of one point as adequate definition of the streamwise position. Spatial resolution errors were minimized by configuring the optics such that the largest possible image displacement was slightly less than the length of the pixel array. The light-level threshold was then set to trigger the data flag on the dark image of the shock wave. The time interval that elapsed between the scan clock pulse and the shock-triggered data flag was proportional to the instantaneous shock position and was converted to an analog signal by a circuit illustrated in Fig. 2 and described below.

An off-the-shelf counter-timer was used to output a digital marker signal, set by the scan clock pulse and reset by the digital data flag. Since this process is repeated in each cycle, the marker contains the shock-position information in pulse-width-modulated (PWM) form. As illustrated in Fig. 3, the PWM marker is converted into an analog level by integration, and the integrator output is sampled at the trailing edge of the marker signal with a sample-and-hold unit. The output of the sample-and-hold unit is the desired shock-position signal. The integrator is reset by the leading edge of the scan clock pulse, repeating the process at the next leading edge of the PWM marker. The signal has a staircase-like appearance, updated at a rate of 3.9 kHz, and conveniently observed on a storage oscilloscope. The entire electronics pckage could be calibrated by a controlled PWM signal from a function generator.

The relationship between the output voltage e and the shock position x is linear:

$$x = A\,e + B \tag{1}$$

The constants were determined by direct calibration after all optical and electronic adjustments were completed. Vertical

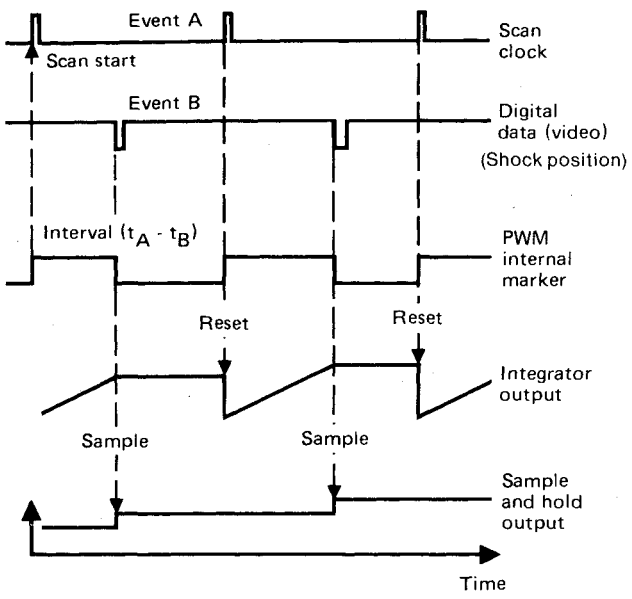

Fig. 3 Timing and control of decoding circuit.

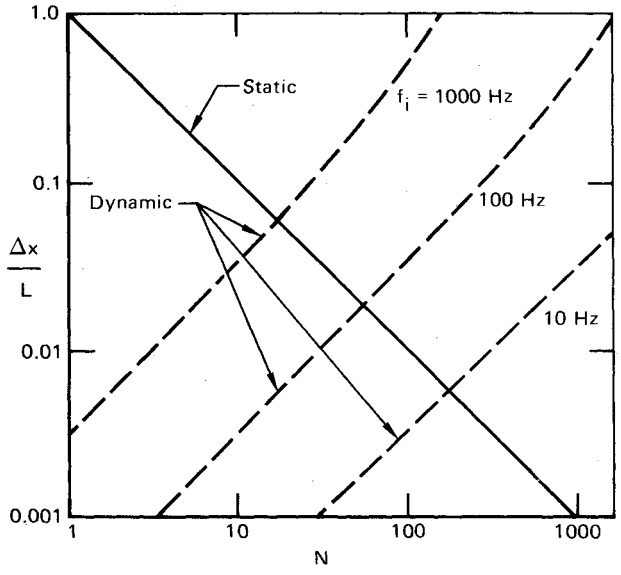

Fig. 4 Static and dynamic errors for an image moving sinusoidally with amplitude $A = L/2$ and frequency f_i.

rods of 1.6-mm diam were placed at known streamwise locations into the field of view, the voltage outputs were manually recorded; and the constants A and B were determined by a least-square fit. The calibrations were executed before and after each run.

System Accuracy

The spatial resolution for a stationary object (Δx_s) is determined primarily by the pixel spacing. The resolution in the image plane is

$$\Delta x_s/L = 1/N \tag{2}$$

where L is the array length (6.35 mm in this case).

If the object is moving, each indicated light-intensity distribution shows a blur whose width is equal to the distance traveled by the shock image between two successive scans. If the image is a sharp, black-to-white boundary moving at a constant speed u, the indicated light-intensity distribution shows a linear variation from low to high level over a distance Δx_b. This distance represents the upper limit of the dynamic error and is given by

$$\frac{\Delta x_b}{L} \leq \frac{N}{(f_s L/u) - N} \tag{3}$$

If the trigger level is set halfway between the high and low levels, the system will yield, in principle, image positions with zero dynamic error. Other trigger levels will result in speed-dependent errors, all less than Δx_b. If the image oscillates sinusoidally with amplitude A and frequency f_i, the maximum blur distance can be estimated using Eq. (3), with $u = 2\pi f_i A$, provided $f_i \ll f_f$. Figure 4 illustrates both types of errors.

The requirements of small static and dynamic uncertainties are conflicting: high spatial resolution means greater blur distance for a given image speed, provided the scan rate f_s (pixels/s) is fixed. Since sensor arrays are available with various pixel numbers, N can be chosen during design for an acceptable compromise. Both errors are referred to the image size; errors in the actual flow are proportional to the ratio of the corresponding linear dimensions of object and the image, as controlled by the optics of the shadowgraph system.

The optical system must be of high quality. Density striations in the test-section walls of commercial mirror glass (used in the first series of tests) introduced light-level variations in the shock-free background that were significant compared to variations typical of shock signatures. Room thermals and a slight drift in camera clock frequency were secondary error sources.

The preceding problems were resolved without undue effort. We consider the system as a viable option for determining the displacement history of any low-speed, visible motion. The method could also be useful in low-speed experiments involving dye- or smoke-visualized, unsteady flows, since the edges of boundary or free shear layers could be detected. The cost of the apparatus is significantly less than that of a general-purpose, two-dimensional image processing system.

Acknowledgment

This research was conducted under the McDonnell Douglas Independent Research and Development Program.

Reference

[1] Chen, C.P., Sajben, M., and Kroutil, J.C., "Shock Wave Oscillations in a Transonic Diffuser Flow," *AIAA Journal* (scheduled for publication in the Sept. 1979 issue).

Rayleigh Scattering Measurements of Time-Resolved Concentration in a Turbulent Propane Jet

T. Michal Dyer*
Sandia Laboratories, Livermore, Calif.

A METHOD has been developed whereby laser Rayleigh scattering is used to determine time- and space-resolved fuel/air concentrations in propane air mixtures. The technique was statically calibrated using prepared homogeneous mixtures in a closed vessel, then was applied to concentration fluctuation measurements in a turbulent,

Received Feb. 20, 1979.

Index categories: Combustion and Combustor Designs; Jets, Wakes and Viscid-Inviscid Flow Interactions; Research Facilities and Instrumentation.

*Member Technical Staff, Combustion Applications Division.